The Impact of the Ground Irregular Sedimentary Structure on the Seismic Motion Amplification Characteristics

A case study in Tottori, Japan

Takashi Nagao
Research Center for Urban Safety and Security, Kobe University, Japan
nagao@people.kobe-u.ac.jp (corresponding author)

Xiao Ma
Graduate School of Engineering, Kobe University, Japan
antarctic96@outlook.com

Received: 16 February 2023 | Revised: 7 April 2023 | Accepted: 15 April 2023

 DOI: https://doi.org/10.48084/etasr.5785

ABSTRACT

The amplification characteristics of seismic motion are determined by the ground structure. In design practice, the ground is assumed to be horizontally stratified. However, the actual ground forms irregular sedimentary structures and the propagation direction of the seismic motion in the soil changes in a complicated way. Thus, the actual amplification factor of seismic motion is dramatically different from the value assumed in design practice. This phenomenon is called the multidimensional effect. The present study targeted at a seismic observation point in Tottori Prefecture, Japan, and estimated the irregular ground structures based on the microtremor observation results. With this ground structure model, Finite Element Analysis (FEA) was conducted and the amplification factors were compared with those determined assuming horizontal stratification. When there is no ground nonlinearity, the multidimensional effect of the ground was more notable in points with thick sedimentary strata, where the peak amplification factor according to the FEA was 1.9 to 3.6 times larger than when horizontal stratification was assumed. In points with thin sedimentary strata, the peak amplification factor ratio was 2.1–2.4. First-order peak frequency was different between cases with irregular ground structures and with horizontal stratification. Furthermore, when the nonlinearity of the ground was evident, the multidimensional effect on the peak amplification factor was not as noticeable as when the ground behaved linearly. The peak magnification ratio due to the multidimensional effect was found to be 2.3. The results of this study show that the amplification characteristics of the seismic motion considered in design practice are likely to be on the dangerous side when the ground is not horizontally stratified.

Keywords-seismic motion; site amplification factor; finite element analysis; ground nonlinearity

I. INTRODUCTION

Seismic motions are determined by the source, path, and site amplification characteristics. Site amplification characteristics display the property of seismic motion being amplified as it propagates through sedimentary grounds, and its amplification factor varies by frequency. When the ground has horizontal stratification and the seismic motion is a vertical incident to the ground, site amplification characteristics can be theoretically calculated based on parameters such as the thickness and the shear modulus of each stratum. Such characteristics are simplified in design practice, where the ground type is classified based on the average S-wave velocity of the top 30m (*Vs*30) [1–3] and the natural period of the shallow subsurface [4], and the amplification factor is determined for each ground type.

There are two problems with such simplification of site amplification characteristics. First, grounds consist of shallow and deep subsurfaces, yet in a simplified assessment, only the influence of the shallow subsurface is considered. The deep subsurface has high rigidity and does not exhibit nonlinear characteristics even during a massive earthquake. In contrast, the shallow subsurface has relatively low rigidity, impacted by nonlinearity during massive earthquakes. The boundary between the two is the engineering bedrock, whose S-wave velocity is 300m/s or higher. The amplification factor for the seismic motion is much higher for the deep subsurface than for the shallow subsurface [5–7]. Even points that are classified in

the same ground type in design practice present notable variations in the amplification factor of seismic motion. However, in the classification based on the amplification characteristics of the deep subsurface, such variations are reduced [8]. Even if the deep subsurface is considered, the theoretical amplification factor calculated with the assumed horizontal stratification is extremely smaller than the one assessed by spectral inversion [9–11] using seismic records [6, 7]. The actual ground structure does not have horizontal stratification and the thickness of each stratum changes in a complex manner for each location. Therefore, changes in the propagation direction of the seismic motion in the ground are complex. As the wave motions are superimposed in the ground in a complex manner, the amplification factor observed on the ground surface becomes notably different from the theoretical value calculated with the assumption of horizontal stratification. This phenomenon is called the multidimensional effect. When the seismic response is evaluated with a one-dimensional (1D) model based on the horizontal stratification, there are notable errors compared to the observed seismic motion [12]. Yet, only a few studies have examined the actual impact of the multidimensional effect of the ground on the amplification factor of the seismic motion. For example, some studies considered a simple two-layer structure with an inclined bedrock, and examined the difference in the seismic response on the ground surface using two-dimensional (2D) models [13, 14]. Another study prepared a 2D model for a multi-layer irregular ground and examined the differences in amplification characteristics [15]. Since the site amplification characteristics dramatically vary by location [16], site amplification characteristics must be accurately evaluated for each point.

In the present study, focus was given on a seismic observation point in Tottori Prefecture, Japan, and site amplification characteristics that consider the impact of deep subsurface at the target point were calculated by using the seismic records observed at that point and in the surrounding areas. Microtremor observation was concucted in the target area to estimate the ground structure around the target point. Then, 2D Finite Element Analysis (FEA) was conducted for the estimated ground structure, and the impact of the irregular sedimentary structures of the ground on the amplification factor of the seismic motion was discussed. To the best of our knowledge, no previous studies have discussed the multidimensional effects in the conditions of both linear and nonlinear responses of the ground, however, this study discusses these effects in both conditions.

II. TARGET POINT AND THE GROUND STRUCTURE

A. Site Amplification Characteristics of the Target Point

The case study was conducted at a point in Tottori Prefecture from the strong-motion seismograph networks K-NET of Japan [17], namely the point TTR004 (Figure 1). With K-NET, S-wave velocity structure down to 20m at a seismic observation point is obtained with P-S logging [18]. The seismic observation point for TTR004 was moved in 2003, and site amplification characteristics for the current observation point have not been obtained so far. Thus, we used seismic records for TTR004 and three K-NET observation points around TTR004 for which site amplification characteristics have been calculated through spectral inversion (TTR002, TTR005, and TTR006) to assess the site amplification characteristics of TTR004. Since earthquakes of higher magnitude (M) have more complex source characteristics, we only studied earthquakes between 4.2 and 6.0 M. To avoid the impact of nonlinear response of the shallow subsurface, we used the records with Peak Ground Acceleration (PGA) of $1m/s^2$ or lower. Since seismic records with low acceleration can have poor Signal-to-Noise Ratio (SN ratio), based on the ω^{-2} rule [19], we selected records with good SN ratio, greater than 0.2Hz. Under the aforementioned conditions, we prepared a set of records for 10 earthquakes. Site amplification characteristics at TTR004 were calculated with (1) based on the spectral ratio of seismic record [20].

$$G_T(f) = G_R(f) \cdot \frac{O_T(f)}{O_R(f)} \cdot \frac{r_T}{r_R} \cdot \frac{\exp\left\{-\left(\pi f r_R\right)/\left(Q(f)Vs\right)\right\}}{\exp\left\{-\left(\pi f r_T\right)/\left(Q(f)Vs\right)\right\}} \quad (1)$$

where $G(f)$ represents the site amplification characteristics, $O(f)$ is the observed seismic motion, r is the hypocentral distance, $Q(f)$ is the quality factor along the propagation path, V_S is the S-wave velocity along the propagation path (3.55km/s in this study based on [21]), and f is the frequency. Subscripts R and T indicate reference and target points (TTR004), respectively. Q is an index that expresses anelastic attenuation with frequency dependence, which varies by each area [22, 23]. In this study, Q was calculated with (2) based on [24]:

$$Q(f) = 152 f^{0.38} \quad (2)$$

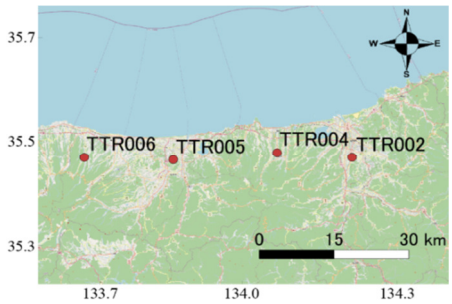

Fig. 1. Target point.

Figure 2 shows the calculated site amplification characteristics. The thin gray line represents site amplification characteristics from individual records, while the red line represents the average. For reference, the site amplification characteristics of TTR004 obtained from the seismic observation records of the previous location through spectral inversion are represented by the blue line. At the previous location, the amplification factor was approximately 1 to 4 and did not show any notable difference based on frequency. However, at the present point, it shows a large amplification factor of 22.7 at 1.3Hz. Though the distance between the previous and the present seismic observation point is only 1.3km, the site amplification characteristics are notably different, therefore, site-specific assessment of amplification factor is extremely important.

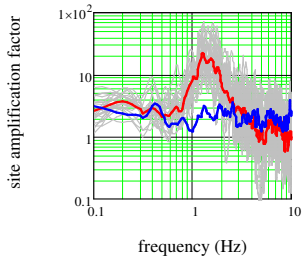

Fig. 2. Site amplification characteristics for TTR004.

B. Estimation of the Ground Structure through Microtremor Observation

We observed the microtremors around TTR004. From the observation result, we calculated the spectral ratio for the horizontal and vertical components of microtremors (H/V spectrum). When surface waves are dominant in microtremors, the H/V spectrum can be considered to be the same with that of the surface waves. Since the surface waves with vertical components are Rayleigh waves, their H/V spectrum can be considered the one of Rayleigh waves [25]. The peak frequency of the H/V spectrum of Rayleigh waves is quite consistent with the first-order peak frequency of the amplification characteristics of seismic motion [26]. Thus, the H/V spectrum is useful as a basis for estimating the ground structure for the microtremor observation points. By assuming the S-wave velocity structure of the ground, the theoretical H/V spectrum for the fundamental-mode Rayleigh waves can be calculated [27]. Thus, from the perspective of minimizing the residual difference between the H/V spectrum and the H/V spectrum of the fundamental-mode Rayleigh waves, the S-wave velocity structure of each point can be estimated.

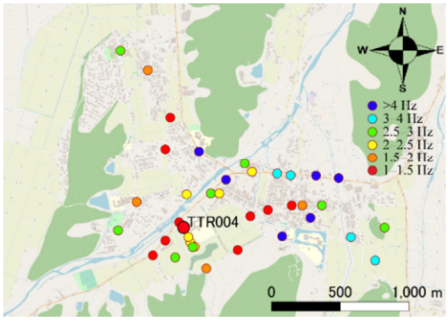

Fig. 3. Microtremor observation points.

Figure 3 shows the observation point locations and the peak frequency of the H/V spectrum as well. The microtremor observations were conducted in the area 2.0km in east–west and 1.5km in north–south. The peak frequency of the H/V spectrum range between 1.0 and 6.5Hz, showing a notable difference in location. This indicates that the ground structure shows notable difference between locations. Figure 4 shows the target survey line for FEA along with the peak frequency of the H/V spectrum. A-H in the Figure are analytical target points of the FEA discussed below, where D refers to TTR004. The survey line width was 600m and the peak frequency was distributed over a wide band of 1.2–3.0Hz as shown below, indicating that even in a narrow range around TTR004, the ground structure rapidly changes.

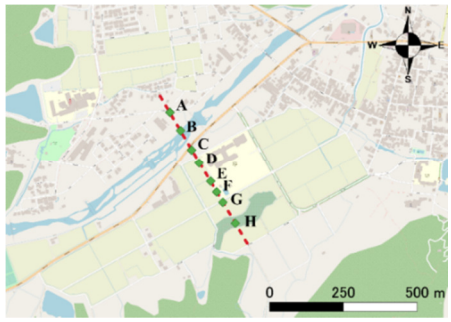

Fig. 4. FEA target survey line.

To calculate the H/V spectrum of the Rayleigh waves, thickness, S-wave velocity, P-wave velocity, and density of each stratum are necessary. By combining the S-wave velocity distribution for the top 20m at TTR004 and that distribution at the depth from J-SHIS [28], the S-wave velocity structure down to deep subsurface can be set. Regarding the S-wave velocity of the top 20m, we also referred to [29]. P-wave velocity and density can be calculated with [30]:

$$\rho = 1.7 + 0.32 \times 10^{-3} V_S \quad (3)$$

$$V_P = 100\sqrt{V_S} \quad (4)$$

where ρ is the density (t/m^3), V_S is the S-wave velocity (m/s), and V_P is the P-wave velocity (m/s).

The ground model was adjusted so that the peak frequencies for the H/V spectrum of the fundamental-mode Rayleigh waves and microtremors would be consistent. For four microtremor observation points on the target survey line of FEA, we changed the thickness of each stratum based on the S-wave velocity structure of TTR004, so that the peak frequency of the H/V spectrum of the microtremors and that of the Rayleigh waves would be consistent. The red line in Figure 5 denotes the H/V spectrum of microtremors and the blue line shows the H/V spectrum of Rayleigh waves. As for the northern edge of the FEA observation line, we were unable to conduct microtremor observation. Therefore, we postulated the peak frequency to be 1.9Hz, which is the mean peak frequency of the H/V spectrum at the two closest points. For the points other than the S-wave velocity structure estimation points, we assumed that the strata thickness would transform linearly, and estimated the ground structure for the target survey line for FEA. Figure 6 and Table I show the obtained ground structure. The thickness of the strata deeper than *Vs* = 800m/s was constant, while the thickness of the strata with *Vs* = 400m/s changed dramatically depending on location. Furthermore, strata with low rigidity of *Vs* = 190m/s were assumed to be limited to the areas A to E, located on the north side of the survey line. Figure 6 also shows the FE mesh. The point C is the point in where the sedimentary strata are at their thickest, while the point G is where they are thinnest. The bedrock depth difference between the two points was 14m.

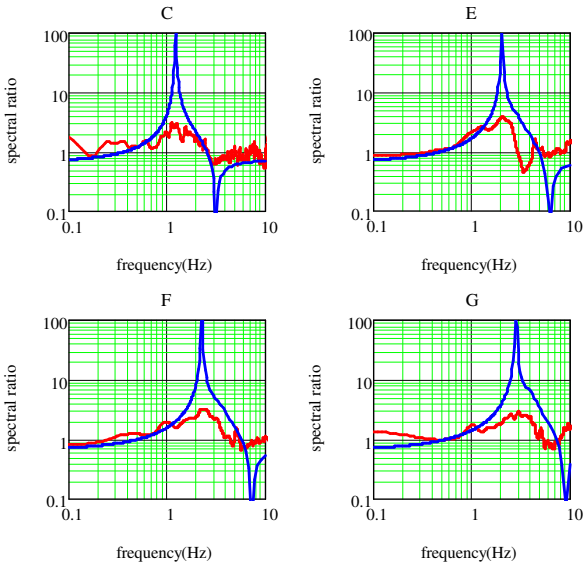

Fig. 5. H/V spectrum.

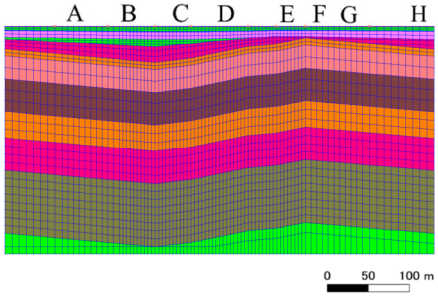

Fig. 6. The ground structure and FE mesh.

TABLE I. STRATUM THICKNESS

Stratum no.	*Vs* (m/s)	A	B	C	D	E	F	G	H
1	180	1							
2	270	4.6	5.4	6	6	5	4	4	4.5
3	200	1							
4	280	9.3	9.6	10	10	9	8	8	9.5
5	190	5.3	7.8	10	6	0.5	0		
6	400	16	19.2	22	20	11	10	2	7.8
7	800	10							
8	1100	32							
9	1400	45							
10	1700	37							
11	2100	46							
12	2700	88							
13	3100	–							

A - H are locations shown in Figure 6. Unit: m.

C. Seismic Response Analysis

To examine the multidimensional effect, we performed 2D FEA for the ground shown in Figure 6. The FEA model has width and height of 600m 320m, respectively. The width of the FEA model was set as the width at which the seismic responses of the output points (i.e. A and H) at both ends were unaffected by the model lateral boundary. The FEA code used was FLIP [31]. The FE mesh height was set such that the seismic motion up to 10Hz could be propagated. The boundary conditions were: during the self-weight analysis, the bottom boundary was fixed and the side boundaries were horizontally fixed while vertically free. During the dynamic analysis, side and bottom boundaries were viscous boundaries. The shallow subsurfaces linearly respond during small earthquakes. However, they could become nonlinear during a massive earthquake. Site amplification characteristics shown in Figure 2 are those where there is no impact of the ground nonlinearity. On the other hand, deep subsurfaces do not exhibit nonlinear characteristics even during a massive earthquake. Thus, deep subsurfaces were modeled with linear planar elements while shallow subsurfaces were either modeled with linear planar elements or elements that can consider the nonlinearity of the ground. Regarding the linear planar elements, the Young's modulus was calculated as:

$$G = \rho V_S^{\,2} \tag{5}$$

$$E = 2(1+\nu)G \tag{6}$$

where G is the shear modulus (kPa), ρ is the density (t/m^3), V_S is the S-wave velocity (m/s), E is the Young's modulus (kPa), and ν is the Poisson's ratio (= 0.33).

Hysteresis damping was set as in (7) [31] and was expressed with Rayleigh damping. Rayleigh damping is expressed with (8). In this study, we set the parameters α and β such that, in the range of 1–5Hz, where the peak frequency of amplification characteristics exists, the residual sum of squares of (7) and (8) would be minimum.

$$\xi = \frac{5.333}{V_S + 66.77} \tag{7}$$

$$\xi = \frac{\alpha}{2\omega} + \frac{\beta\omega}{2} \tag{8}$$

where ξ is the damping constant, V_S is the S-wave velocity (m/s), α and β are the parameters that multiply the mass matrix and rigidity matrix respectively, and ω is the angular frequency ($= 2\pi f$).

When considering the nonlinearity of the ground, we employed multi-spring elements that can assess responses during principal stress axes rotation [32] for layers of *Vs* = 400m/s or less. For the nonlinearity of the ground, we used the hyperbolic model below [33].

$$\frac{G_m}{G_0} = \frac{1}{1+\frac{G_0\gamma}{\tau_m}} \tag{9}$$

where G_m is the shear modulus, G_0 is the initial shear modulus, γ is the shear strain, and τ_m is the shear strength, which is calculated by (10) [34]. Shear modulus G_m of the ground at each depth is calculated with the reference shear modulus and the reference effective confining pressure using (11) [35]. The reference bulk modulus K_{ma} is calculated with (12).

$$\tau_m = \sigma_m' \sin\phi \tag{10}$$

$$G_m = G_{ma}\left(\frac{\sigma_m'}{\sigma_{ma}'}\right)^{0.5} \quad (11)$$

$$K_{ma} = \frac{2}{3}\left(\frac{1+\nu}{1-2\nu}\right)G_{ma} \quad (12)$$

where G_{ma} is the reference shear modulus, σ_m' is the effective confining pressure, σ_{ma}' is the reference effective confining pressure that corresponds to the reference shear modulus, ϕ is the shear resistance angle, and ν is the Poisson's ratio.

Tables II and III show the ground parameters used for FEA for linear response and nonlinear response, respectively.

TABLE II. GROUND PARAMETERS (LINEAR RESPONSE)

Stratum No.	*Vs* (m/s)	ρ (t/m^3)	*E* (kPa)	α	β
1	180	1.8	152089	0.1	0.002
2	270	1.8	361212	0.1	0.001
3	200	1.8	198196	0.1	0.002
4	280	1.8	408910	0.1	0.001
5	190	1.8	178872	0.1	0.002
6	400	1.8	834510	0.098	0.001
7	800	2.0	3264600	0.1	0
8	1100	2.1	6475050	0.1	0
9	1400	2.2	10979200	0.089	0
10	1700	2.4	16912300	0.073	0
11	2100	2.4	27279400	0.06	0
12	2700	2.6	48744500	0.043	0
13	3100	2.7	67465200	0.041	0

TABLE III. GROUND PARAMETERS (NONLINEAR RESPONSE)

Stratum No.	*Vs* (m/s)	ρ (t/m^3)	σ_{ma}' (kPa)	G_{ma} (kPa)	K_{ma} (kPa)
1	180	1.8	6.62	58320	152089
2	270	1.8	55.13	138510	361212
3	200	1.8	104.0	76000	198196
4	280	1.8	184.5	156800	408910
5	190	1.8	299.8	68590	178872
6	400	1.8	488.8	320000	834510

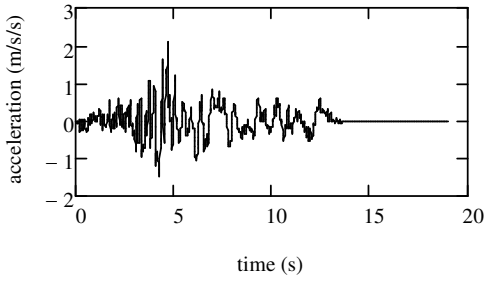

Fig. 7. Seismic waveform.

We used incident seismic waveform at the engineering bedrock by deconvolution [37] based on the seismic waveform observed at the Hachinohe Port during the Tokachi-Oki earthquake in 1968 (Figure 7). The PGA was 2.1m/s^2 and the dominant frequencies were 0.4 and 1.0Hz. The seismic motion in the low frequency range has an impact on the nonlinearity of the ground [38]. In this study, we used the seismic waveform shown in Figure 7 and the 0.1m/s^2 PGA waveform in order to avoid the impact of ground nonlinearity. The evaluated amplification characteristics in 2D FEA (hereafter 2D amplification characteristics) were the spectral ratio of the seismic motion at the ground surface and the input seismic motion. When obtaining the spectral ratio, the seismic motions were both smoothed with the Parzen Window [39] with a band width of 0.2Hz. The output points of FEA are the 8 points, from A to H, shown in Figure 6. To discuss the multidimensional effect of the ground, we evaluated the amplification characteristics under horizontal stratification structure (hereafter referred to as the 1D amplification characteristics). When the surface ground nonlinearity was not considered, the evaluation was performed based on the multiple reflection theory. When it was considered, we used 1D FEA with the same ground parameters as the 2D FEA. The evaluation of the amplification characteristics using the multiple reflection theory was expressed with Rayleigh damping, with the same values as the linear planar element damping in FEA.

III. RESULTS AND DISCUSSION

The conditions without an impact of the ground nonlinearity where the PGA of the input seismic motion is 0.1m/s^2 is discussed first. Figure 8 shows the acceleration time history for point C where the thickness of sedimentary strata is at its thickest. The 1D and 2D responses are indicated with blue and red lines, respectively. Ground surface PGA in 1D analysis and 2D analysis were 0.27 and 0.62 m/s^2, respectively. It is noted that the PGA of the 2D analysis was 2.3 times that of the 1D analysis, indicating the multidimensional effect. As for the seismic waveform envelope, while the 1D response was similar to the input waveform, the 2D response was different from the input waveform, where the maximum response appeared in 6.94s and the duration of the seismic motion was long. It is a result of complex and repetitive seismic-wave incidences and reflections on each stratum.

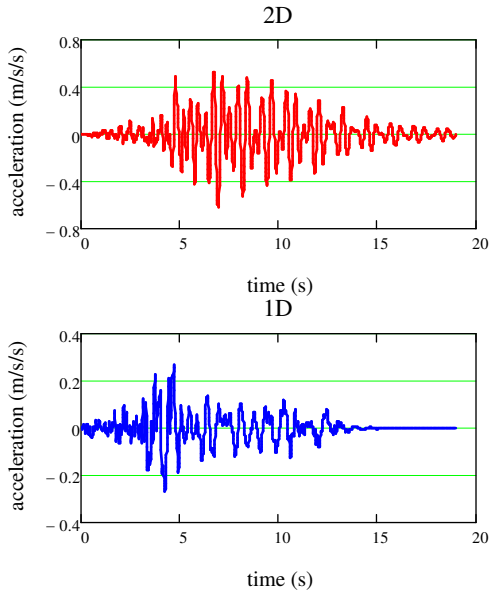

Fig. 8. Response at point C (linear response).

Figure 9 shows the amplification characteristics of each point. The blue line indicates the 1D response and the red line the 2D response. At points A to D with thick sedimentary strata, the difference between 2D and 1D amplification characteristics was notable. The peak magnification for 2D and 1D amplification characteristics ranged from 14.9 to 35.8, and from 7.8 to 10.0, respectively. The magnification ratio of both was in the range of 1.9 and 3.6. The peak magnification ratio was the largest at point C where the sedimentary strata were the thickest. At point D, which is equivalent to TTR004, the peak magnification of 2D amplification characteristics was 17.6, mostly reproducing the peak magnification of site amplification characteristics (22.7) shown in Figure 2. In contrast, with 1D amplification characteristics, the peak magnification was 8.9, not reproducing the actual amplification factor.

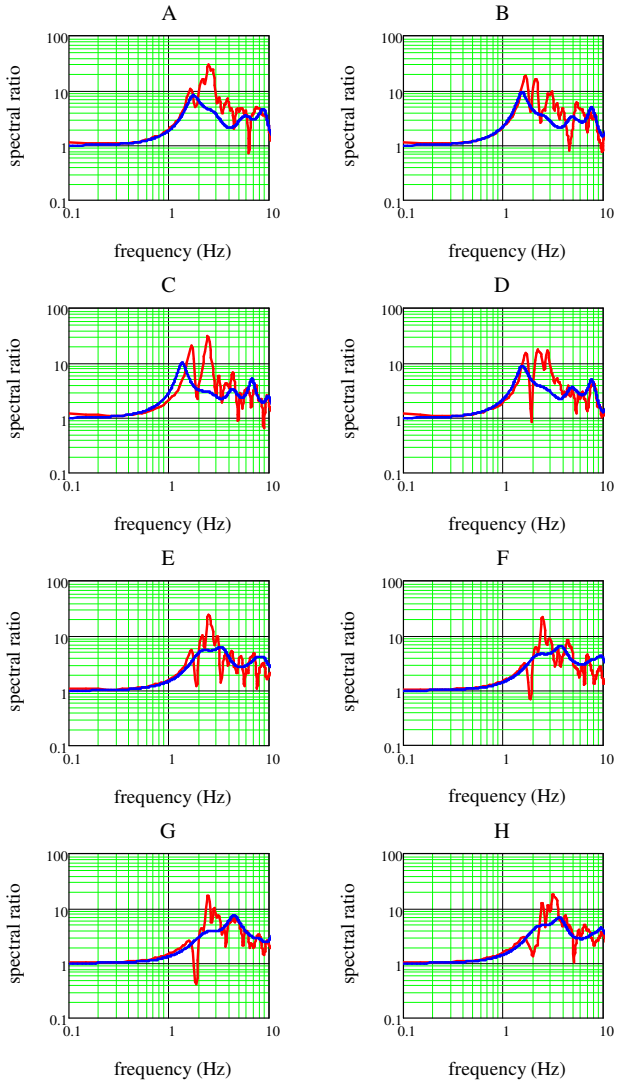

Fig. 9. Comparison of the amplification characteristics (linear response).

Regarding the peak frequency, there was a difference between 1D and 2D amplification characteristics. With 2D amplification characteristics, the first-order peak frequency ranged from 1.6 to 1.7Hz, but with 1D amplification characteristics, it ranged from 1.4 to 1.8Hz. Thus, in 2D amplification characteristics, the first-order peak frequency appears at frequencies higher than in 1D amplification characteristics, because the seismic response at each point is impacted not only by the ground structure immediately below, but also by the surrounding ground structures. However, at point A, the first-order peak frequency was almost the same for both 2D and 1D amplification characteristics.

For points E to H with thin sedimentary strata, the difference between 2D and 1D amplification characteristics was limited, even though the multidimensional effect was confirmed. In other words, the peak magnification ranged in the range of 5.4 to 7.3 and 1.2 to 17.5, respectively, for 1D and 2D amplification characteristics. The magnification ratio of both was in the range of 2.1 to 2.4. The first-order peak frequency ranged from 2.2 to 3.4Hz for 1D amplification characteristics, though not clear for point E. For 2D amplification characteristics, it ranged betweeen 1.6 and 2.5Hz. The first-order peak frequency for 2D amplification characteristics was lower than that for 1D amplification characteristics. This is also a result of the impact of the surrounding ground structures on the seismic motion amplification characteristics at each point caused by the multidimensional effect.

Next, a case in which there is an impact of the ground nonlinearity and the PGA of the input seismic motion is 2.1m/s^2 is discussed. Figure 10 shows the acceleration time history for point C where the sedimentary strata were the thickest. 1D and 2D response are indicated with blue and red lines, respectively.

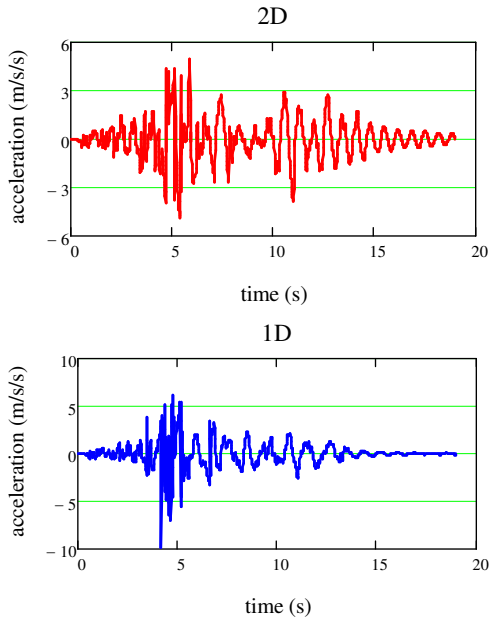

Fig. 10. Response at point C (nonlinear response)

The surface ground experience reduced rigidity and increased damping when the ground becamee nonlinear due to the strong seismic motion. Thus, the first-order peak frequency decreases and the amplification factor also decreases.

Therefore, each amplification characteristic is different from those of linear response. First, with the ground surface PGA with 1D response of 9.92m/s^2, 2D response was smaller at 4.95m/s^2. Due to the multidimensional effect, the superposition of the waveform occurred in 2D response, but the PGA became smaller than that of the 1D response due to the soil nonlinearity. The acceleration of the 1D response reached its maximum in 4.2s, a response with high frequency. In contrast, in the 2D response, the maximum was reached in 5.9s. Similar to the linear response, the time for the maximum acceleration response of the ground surface was different due to the multidimensional effect. Furthermore, with the 1D response, as the amplitude of the input seismic motion decreased, the amplitude of the ground surface response decreased. After 5s, the amplitude decreased dramatically. In contrast, with the 2D response, even if the amplitude of the input seismic motion decreased, the response would remained larger and the duration was long. This is the same as in the linear response.

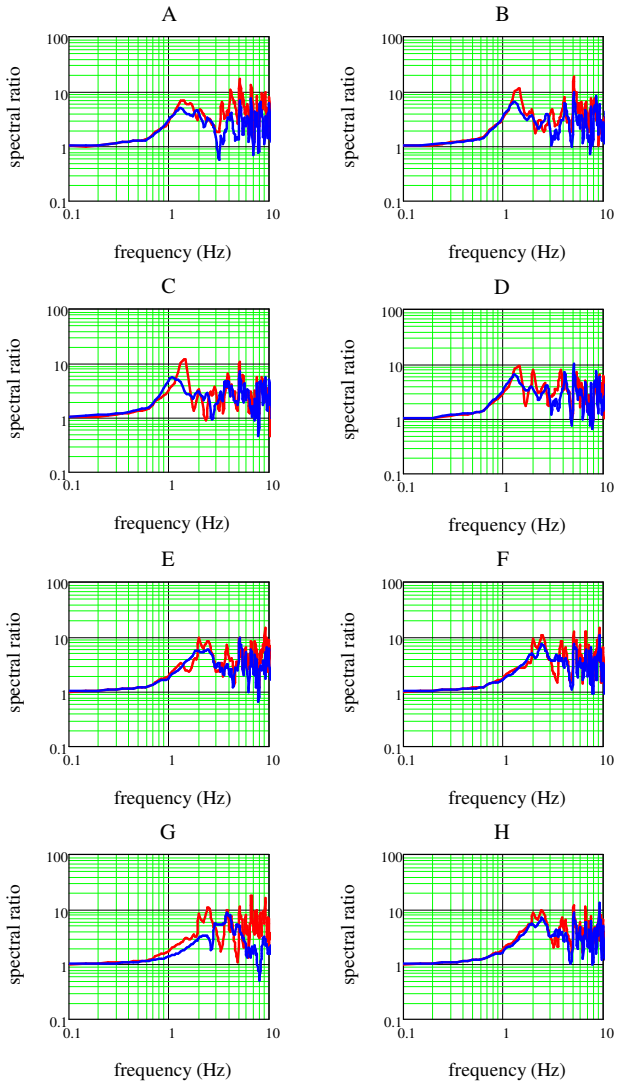

Fig. 11. Comparison of amplification characteristics (nonlinear response).

In Figure 11, 1D amplification characteristics are indicated in blue and 2D amplification characteristics in red. Regarding the peak magnification, the difference between 2D and 1D amplification characteristics decreased compared to the case without the impact of the ground nonlinearity. The same trend can be seen in all points. 2D amplification characteristics had a peak magnification that was 1.4 to 2.3 times more than that of the 1D amplification characteristics. Same as in the case of ground with a linear response, point C with the thickest sedimentary strata had the largest peak magnification. As for the first-order peak frequency, points A to D with the thick sedimentary strata had a less difference between 2D and 1D amplification characteristics compared to the linear response. It can be seen that the peak magnification was notably different between 2D and 1D amplification characteristics at all points. The amplification characteristics of seismic motion under the multidimensional effect could not be explained with the horizontal stratification that is usually assumed in design practice. Thus, simplified handling in design practice could lead to highly risky decisions. This trend was especially notable in points with thick sedimentary strata.

As a next step, we compare the present results with those of previous studies that examined the multidimensional effect [13–15]. Regarding the S-wave velocity of the bedrock in consideration, in contrast to the present 3100m/s, the past studies had values in the range of 800–2000m/s. The previous studies did not discuss the multidimensional effect for all deep ground structures. While the inclination angle of the bedrock in the present study was 20°, past studies considered 30° or higher, meaning that they handled conditions where the multidimensional effect was more likely to occur. As for the nonlinearity of the surface ground, no past study considered both linear and nonlinear cases as the present one does. Though there are differences in the conditions, the ratio of the peak magnification for 2D amplification characteristics that consider irregular sedimentary structure of the ground and 1D amplification characteristics was in the range of 0.7–1.9 in the previous studies. However, in the present study, when the ground nonlinearity was not considered, it was as high as 3.6, and when it was, it was 2.3 at maximum. Thus, larger magnification ratio than past studies was obtained due to the multidimensional effect of the ground. The reason for this is that, as discussed above, we considered the ground with S-wave velocity up to 3100m/s. The difference in the peak frequency between 2D and 1D amplification characteristics has been examined in the past, but the difference in specific frequency varies based on the ground conditions.

IV. CONCLUSIONS

In the current study, the amplification characteristics of seismic motion were analyzed at a seismic observation point in Tottori Prefecture, Japan, where the ground structure dramatically changes in a narrow area. Then, we compared them with the amplification characteristics of a horizontal stratification ground structure that is usually considered in design practice. The main drawn conclusions are:

- At points where the ground structure is irregular, the site amplification characteristics evaluated using a seismic record have a larger peak magnification than that assumed

by horizontal stratification. Thus, the amplification characteristics of the actual seismic motion cannot be explained with the horizontal stratification that is usually assumed in design practice. FEA that considers irregular ground structure can mostly assess the peak magnification of site amplification characteristics based on seismic records.

- When there is no ground nonlinearity, points with thick sedimentary strata had higher multidimensional effects, where the peak magnification of 2D amplification characteristics was 1.9–3.6 times higher than that from 1D amplification characteristics. Alternatively, at points with thin sedimentary strata, the difference between the two was relatively small, e.g. the 2D amplification characteristics were only 2.1–2.4 times higher than 1D amplification characteristics. As for the first-order peak frequency, with irregular ground structures, there is an impact of the surrounding ground structures. Therefore, the frequency is different from the one acquired when horizontal stratification is assumed.
- When there is ground nonlinearity, the multidimensional effect on the peak magnification of site amplification characteristics was less notable than when the ground behaved linearly. However, at points with thick sedimentary strata, the peak magnification of 2D amplification characteristics was 2.3 times higher than that of 1D amplification characteristics.

ACKNOWLEDGEMENT

We received support from Yasuhiro Fukushima and Tianyue Hu for the microtremor observation. We used the seismic records published by K-NET.

REFERENCES

[1] *EN 1998-1:2004: Eurocode 8: Design of structures for earthquake resistance – Part 1: General rules, seismic actions and rules for buildings. Brussels, Belgium: CEN, 2004.*

[2] *FEMA 368, NEHRP recommended provisions for seismic regulations for new buildings and other structures, 2000 Edition. Washington, DC: Building Seismic Safety Council for the Federal Emergency Management Agency, 2001.*

[3] *AASHTO, Guide Specifications for LRFD Seismic Bridge Design, 2nd Edition. Washington, DC, USA: American Association of State Highway and Transportation, 2014.*

[4] *Specifications for highway bridges, part5, Seismic design, ver. 2012. Japan Road Association, Maruzen Co., Ltd., 2016.*

[5] T. Nagao, "Seismic Amplification by Deep Subsurface and Proposal of a New Proxy," *Engineering, Technology & Applied Science Research*, vol. 10, no. 1, pp. 5157–5163, Feb. 2020, https://doi.org/10.48084/etasr.3276.

[6] T. Nagao and Y. Fukushima, "Source- and Site-Specific Earthquake Ground Motions: Application of a State-of-the-Art Evaluation Method," *Engineering, Technology & Applied Science Research*, vol. 10, no. 4, pp. 5882–5888, Aug. 2020, https://doi.org/10.48084/etasr.3612.

[7] Y. Fukushima, T. Nagao, J. Oshige, and I. Suetomi, "Ground motion evaluation for intra-plate earthquake by different site amplification factors and source models," in *7th International Conference on Earthquake Geotechnical Engineering*, Rome, Italy, Jun. 2019, pp. 2484–2492.

[8] T. Nagao, "Maximum Credible Earthquake Ground Motions with Focus on Site Amplification due to Deep Subsurface," *Engineering, Technology & Applied Science Research*, vol. 11, no. 2, pp. 6873–6881, Apr. 2021, https://doi.org/10.48084/etasr.3991.

[9] D. J. Andrews, "Objective Determination of Source Parameters and Similarity of Earthquakes of Different Size," in *Earthquake Source Mechanics*, Washington, DC, USA: American Geophysical Union, 1986, pp. 259–267.

[10] T. Iwata and K. Irikura, "Source parameters of the 1983 Japan Sea earthquake sequence.," *Journal of Physics of the Earth*, vol. 36, no. 4, pp. 155–184, 1988, https://doi.org/10.4294/jpe1952.36.155.

[11] J. Boatwright, J. B. Fletcher, and T. E. Fumal, "A general inversion scheme for source, site, and propagation characteristics using multiply recorded sets of moderate-sized earthquakes," *Bulletin of the Seismological Society of America*, vol. 81, no. 5, pp. 1754–1782, Oct. 1991, https://doi.org/10.1785/BSSA0810051754.

[12] E. M. Thompson, L. G. Baise, Y. Tanaka, and R. E. Kayen, "A taxonomy of site response complexity," *Soil Dynamics and Earthquake Engineering*, vol. 41, pp. 32–43, Oct. 2012, https://doi.org/10.1016/j.soildyn.2012.04.005.

[13] P. P. Bruno, E. Carrara, V. di Fiore, A. Rapolla, and N. Roberti, "Seismic site amplification factor (DAF): Geometrical limits of 1D modelling," in *4th EEGS Meeting*, Barcelona, Spain, Sep. 1998, https://doi.org/10.3997/2214-4609.201407182.

[14] K. Pitilakis, E. Riga, A. Anastasiadis, and K. Makra, "New elastic spectra, site amplification factors and aggravation factors for complex subsurface geometry towards the improvement of EC8," in *6th International Conference on Earthquake Geotechnical Engineering*, Christchurch, New Zealand, Nov. 2015, pp. 1–20.

[15] O.-J. Ktenidou, D. Raptakis, P. Apostolidis, and K. Pitilakis, "Aspects of Surface Topography and Site Effects - Experimental and Numerical Studies at Aegion, Greece," in *4th International Conference on Earthquake Geotechnical Engineering*, Thessaloniki, Greece, Jun. 2007.

[16] T. Nagao, "Variation Evaluation of Path Characteristic and Site Amplification Factor of Earthquake Ground Motion at Four Sites in Central Japan," *Engineering, Technology & Applied Science Research*, vol. 11, no. 5, pp. 7658–7664, Oct. 2021, https://doi.org/10.48084/etasr.4405.

[17] S. Kinoshita, "Kyoshin Net (K-NET)," *Seismological Research Letters*, vol. 69, no. 4, pp. 309–332, Jul. 1998, https://doi.org/10.1785/gssrl.69.4.309.

[18] "Strong-motion seismograph networks (K-NET, KiK-net)," *Bosai*. https://www.kyoshin.bosai.go.jp.

[19] K. Aki, "Scaling law of seismic spectrum," *Journal of Geophysical Research*, vol. 72, no. 4, pp. 1217–1231, 1967, https://doi.org/10.1029/JZ072i004p01217.

[20] Y. Fukushima and T. Nagao, "Variation of Earthquake Ground Motions with Focus on Site Amplification Factors: A Case Study," *Engineering, Technology & Applied Science Research*, vol. 9, no. 4, pp. 4355–4360, Aug. 2019, https://doi.org/10.48084/etasr.2856.

[21] K. Kato, "Evaluation of Source, Path, and Site Amplification Factors from the K-Net Strong Motion Records of the 1997 Kagoshima-Ken-Hokuseibu Earthqltakes," *Journal of Structural and Construction Engineering*, vol. 66, no. 543, pp. 61–68, 2001, https://doi.org/10.3130/aijs.66.61_2.

[22] A. Petukhin, K. Irikura, S. Ohmi, and T. Kagawa, "Estimation of Q-Values in the Seismogenic and Aseismic Layers in the Kinki Region, Japan, by Elimination of the Geometrical Spreading Effect Using Ray Approximation," *Bulletin of the Seismological Society of America*, vol. 93, no. 4, pp. 1498–1515, Aug. 2003, https://doi.org/10.1785/0120020205.

[23] T. Satoh, H. Kawase, and T. Sato, "Statistical spectral model of earthquakes in the eastern Tohoku district, Japan, based on the surface and borehole records observed in Sendai," *Bulletin of the Seismological Society of America*, vol. 87, no. 2, pp. 446–462, Apr. 1997, https://doi.org/10.1785/BSSA0870020446.

[24] T. Satoh and Y. Tatsumi, "Source, path, and site effects for crustal and subduction earthquakesinferred from strong motion records in Japan,"

Journal of Structural and Construction Engineering, vol. 556, pp. 15–24, 2002.

[25] SESAME European research project WP12 – Deliverable D23.12, *Guidelines for the implementation of the H/V spectral ratio technique on ambient vibrations measurements, processing and interpretation*. European Commission – Research General Directorate, 2004.

[26] T. Satoh, H. Kawase, and S. Matsushima, "Differences Between Site Characteristics Obtained From Microtremors, S-waves, P-waves, and Codas," *Bulletin of the Seismological Society of America*, vol. 91, no. 2, pp. 313–334, Apr. 2001, https://doi.org/10.1785/0119990149.

[27] N. A. Haskell, "The dispersion of surface waves on multilayered media," *Bulletin of the Seismological Society of America*, vol. 43, no. 1, pp. 17–34, Jan. 1953, https://doi.org/10.1785/BSSA0430010017.

[28] H. Fujiwara, S. Kawai, K. X. Hao, N. Morikawa, and H. Azuma, "J-SHIS-An integrated system for sharing information on national seismic hazard maps for Japan," in *16th World Conference on Earthquake Engineering*, Santiago, Chile, Jan. 2017.

[29] T. Imai and K. Tonoughi, "Correlation of N value with S-wave velocity and shear modulus," in *Penetration Testing 1*, Boca Raton, FL, USA: CRC Press, 1982, pp. 67–72.

[30] T. Nagao, M. Yamada, and A. Nozu, "A study on the interpretation of wave components in microtremor H/V spectrum," *Journal of Japan Society of Civil Engineers*, vol. 68, no. 1, pp. 48–62, Jan. 2012, https://doi.org/10.2208/jscejseee.68.48.

[31] S. Iai, Y. Matsunaga, and T. Kameoka, "Strain Space Plasticity Model for Cyclic Mobility," *Soils and Foundations*, vol. 32, no. 2, pp. 1–15, Jun. 1992, https://doi.org/10.3208/sandf1972.32.2_1.

[32] J. Bielak, O. Ghattas, and E.-J. Kim, "Parallel Octree-based Finite Element Method for Large-scale Earthquake Ground Motion Simulation," *Computer Modeling in Engineering and Science*, vol. 10, no. 2, pp. 99–112, 2005.

[33] I. Towhata and K. Ishihara, "Modeling soil behavior under principal stress axes rotation," in *5th International Conference on Numerical Methods in Geomechanics*, Nagoya, Japan, Apr. 1985, vol. 1, pp. 523–530.

[34] B. O. Hardin and V. P. Drnevich, "Shear Modulus and Damping in Soils: Design Equations and Curves," *Journal of the Soil Mechanics and Foundations Division*, vol. 98, no. 7, pp. 667–692, Jul. 1972, https://doi.org/10.1061/JSFEAQ.0001760.

[35] T. Morita, S. Iai, H. Liu, K. Ichii, and Y. Sato, "Simplified method to determine parameter of FLIP," Technical Note of the Port and Harbour Research Institute No. 869, 1997.

[36] I. Suetomi and N. Yoshida, "Nonlinear Behavior of Surface Deposit during the 1995 Hyogoken-Nambu Earthquake," *Soils and Foundations*, vol. 38, pp. 11–22, Sep. 1998, https://doi.org/10.3208/sandf.38.Special_11.

[37] I. Towhata, *Geotechnical Earthquake Engineering*. New York, NY, USA: Springer, 2008.

[38] N. Yoshida, *Seismic Ground Response Analysis*, 2015th edition. New York, NY, USA: Springer, 2014.

[39] E. Parzen, "On Estimation of a Probability Density Function and Mode," *The Annals of Mathematical Statistics*, vol. 33, no. 3, pp. 1065–1076, 1962.